# Genotype–phenotype correlations in neonatal epilepsies caused by mutations in the voltage sensor of $K_V7.2$ potassium channel subunits

Francesco Miceli[a], Maria Virginia Soldovieri[b], Paolo Ambrosino[b], Vincenzo Barrese[a], Michele Migliore[c], Maria Roberta Cilio[d,e,1], and Maurizio Taglialatela[a,b,2]

[a]Department of Neuroscience, University of Naples Federico II, 80131 Naples, Italy; [b]Department of Medicine and Health Science, University of Molise, 86100 Campobasso, Italy; [c]Institute of Biophysics, National Research Council, 90146 Palermo, Italy; [d]Division of Neurology, Bambino Gesù Children's Hospital and Research Institute, 00165 Rome, Italy; and [e]Department of Neurology, University of California, San Francisco, CA 94143

Edited* by Ramon Latorre, Centro Interdisciplinario de Neurociencias, Universidad de Valparaíso, Valparaíso, Chile, and approved January 29, 2013 (received for review October 5, 2012)

**Mutations in the $K_V7.2$ gene encoding for voltage-dependent $K^+$ channel subunits cause neonatal epilepsies with wide phenotypic heterogeneity. Two mutations affecting the same positively charged residue in the $S_4$ domain of $K_V7.2$ have been found in children affected with benign familial neonatal seizures (R213W mutation) or with neonatal epileptic encephalopathy with severe pharmacoresistant seizures and neurocognitive delay, suppression-burst pattern at EEG, and distinct neuroradiological features (R213Q mutation). To examine the molecular basis for this strikingly different phenotype, we studied the functional characteristics of mutant channels by using electrophysiological techniques, computational modeling, and homology modeling. Functional studies revealed that, in homomeric or heteromeric configuration with $K_V7.2$ and/or $K_V7.3$ subunits, both mutations markedly destabilized the open state, causing a dramatic decrease in channel voltage sensitivity. These functional changes were (*i*) more pronounced for channels incorporating R213Q- than R213W-carrying $K_V7.2$ subunits; (*ii*) proportional to the number of mutant subunits incorporated; and (*iii*) fully restored by the neuronal $K_v7$ activator retigabine. Homology modeling confirmed a critical role for the R213 residue in stabilizing the activated voltage sensor configuration. Modeling experiments in CA1 hippocampal pyramidal cells revealed that both mutations increased cell firing frequency, with the R213Q mutation prompting more dramatic functional changes compared with the R213W mutation. These results suggest that the clinical disease severity may be related to the extent of the mutation-induced functional $K^+$ channel impairment, and set the preclinical basis for the potential use of $K_v7$ openers as a targeted anticonvulsant therapy to improve developmental outcome in neonates with $K_V7.2$ encephalopathy.**

channelopathies | potassium channel gating | anticonvulsants | π-stacking interaction | brain development

Heteromeric assembly of $K_V7.2$ (KCNQ2) and $K_V7.3$ (KCNQ3) voltage-dependent $K^+$ channel subunits underlies the M-current ($I_{KM}$) (1), a slowly activating and deactivating $K^+$ neuronal current that regulates excitability in the subthreshold range for action potential (AP) generation (2, 3) and is also involved in network oscillation and synchronization control (4).

Mutations in $K_V7.2$ (5, 6) and, more rarely, $K_V7.3$ (7) genes are responsible for benign familial neonatal seizures (BFNS), a rare, autosomal-dominant epilepsy of newborns characterized by recurrent seizures that begin in the very first days of life in otherwise healthy newborns and remit after a few weeks or months; BFNS-affected individuals mostly display normal interictal EEG, neuroimaging findings, and psychomotor development.

More recently, *$K_V7.2$* mutations have been described in neonates affected with pharmacoresistant seizures with psychomotor retardation, suppression-burst pattern at EEG, and distinct neuroradiological features, thus defining a so-called "$K_V7.2$ encephalopathy" (8), as well as in children with Ohtahara syndrome or early infantile epileptic encephalopathy with suppression-burst (9), the most severe and the earliest developing age-related epileptic encephalopathy (10).

In particular, two heterozygous mutations affecting the same positively charged residue (R213) within the $K_V7.2$ $S_4$ transmembrane segment of the voltage-sensing domain (VSD) are associated with neonatal epileptic encephalopathy in a patient with profound mental retardation, asymmetric spastic quadriplegia, and macrocephaly (R213Q) (8, 11), or with typical BFNS (R213W) (12).

To investigate the molecular basis for such dramatically different phenotypes, we studied the biophysical characteristics of channels incorporating $K_V7.2$ R213Q/W mutant subunits in homomeric and heteromeric configuration with various ratios of $K_V7.2$ and/or $K_V7.3$ subunits. The results obtained revealed that both mutations decreased channel voltage sensitivity by reducing the stability of the activated VSD configuration; these gating alterations appeared significantly more pronounced for R213Q- than R213W-incorporating channels, and were fully reversed by the neuronal $K_v7/I_{KM}$ channel activator retigabine (13). Modeling experiments in hippocampal CA1 pyramidal cells whose $I_{KM}$ incorporated the experimentally defined mutation-induced gating changes showed that R213W- and, more so, R213Q-containing heteromeric channels markedly increased neuronal excitability. Finally, analysis of the structural consequences of R213W and R213Q substitutions in a homology-built model of the activated configuration of $K_V7.2$ VSD suggested that, although both mutations impeded the formation of ionized hydrogen bonds between R213 and neighboring negatively charged amino acids, the introduction of a W, but not of a Q, residue at R213 may provide a certain degree of VSD stabilization by creating a unique aromatic staking interaction.

The present results reveal that the extent of mutation-induced functional impairment may be related to the clinical severity of the disease, thus uncovering genotype–phenotype correlations in $K_V7.2$-linked channelopathies that might have relevant impact on disease-management procedures (i.e., for early genotyping), as well as on clinical course prediction and pharmacological treatment.

## Results

**Functional Properties of Homomeric $K_V7.2$ Channels Carrying R213W (R6W) and R213Q (R6Q) Substitutions.** $K_v7$ channels assemble as tetramers, with each subunit displaying a core domain formed by

Author contributions: F.M., M.M., M.R.C., and M.T. designed research; F.M., M.V.S., P.A., V.B., and M.M. performed research; F.M., M.V.S., P.A., V.B., M.M., and M.T. analyzed data; and M.M., M.R.C., and M.T. wrote the paper.

The authors declare no conflict of interest.

*This Direct Submission article had a prearranged editor.

[1]Present address: Division of Epilepsy and Clinical Neurophysiology, Department of Neurology, University of California, San Francisco, CA 94143-0114.

[2]To whom correspondence should be addressed. E-mail: m.taglialatela@unimol.it.

This article contains supporting information online at www.pnas.org/lookup/suppl/doi:10.1073/pnas.1216867110/-/DCSupplemental.

six transmembrane segments ($S_1$–$S_6$), and cytoplasmic N-and C-termini; within each subunit, the $S_1$ to $S_4$ segments form the VSD arranged symmetrically around the pore. $S_4$ shows a variable number of positively charged amino acids (numbered from 0 to 7). Characteristic in all $K_v7$ subunits is the presence of an uncharged Q residue (Q204 in $K_V7.2$) at the position corresponding to R3 in most $K_v$ channels; R213 is the fifth positively charged residue along the $K_V7.2$ $S_4$ segment. To facilitate sequence comparison with other $K_V$ channels whose crystal structures have been determined and that carry a positive charge at R3, the R213 residue in $K_V7.2$ will be referred to as R6, and the R213W and R213Q mutations as R6W and R6Q, respectively (Fig. 1*A*), despite the fact that we previously used the R6 abbreviation for the adjacent R214 residue (11).

Homomeric $K_V7.2$ channels expressed in CHO cells generated voltage-dependent $K^+$-selective currents characterized by a slow time course of activation and deactivation, and a threshold for current activation around −50 mV (Fig. 1*B*). Homomeric $K_V7.2$ R6W and $K_V7.2$ R6Q channels also generated functional voltage-dependent $K^+$ currents that had maximal densities identical to $K_V7.2$ channels (Table 1), but required more depolarized potentials to become activated; indeed, the threshold voltages for current activation were −10 mV in $K_V7.2$ R6W channels and 0 mV in $K_V7.2$ R6Q channels (Fig. 1*B*). The half activation potential ($V_{1/2}$) was −23 mV in $K_V7.2$ channels; this value was right-shifted by 58 mV and 68 mV in R6W and R6Q mutant channels, respectively (Fig. 1*C* and Table 1). For homomeric $K_V7.2$ R6Q channels, these results confirm previous data (11).

$K^+$ currents carried by homomeric $K_V7.2$ channels displayed double-exponential activation kinetics (1, 14), with a voltage-dependent fast time constant ($\tau_f$) and a slow time constant ($\tau_s$) showing little voltage sensitivity between −20 and +60 mV (15). $\tau_f$ relative amplitude accounted for approximately 90% of the total activation process. Compared with $K_V7.2$ channels, currents carried by $K_V7.2$ R6W or $K_V7.2$ R6Q homomeric channels showed no appreciable difference in the weighted average of $\tau_f$ and $\tau_s$ (Fig. 1*D*). By contrast, deactivation kinetics of $K_V7.2$ R6W and, more so, $K_V7.2$ R6Q channels were faster than those recorded from $K_V7.2$ channels (Fig. 1*D*). At the end of a −20 mV step, a significant fraction of $K_V7.2$ channels appeared to still be in the open state; by contrast, more complete deactivation was observed for $K_V7.2$ R6W and $K_V7.2$ R6Q channels, the latter being fully closed at the end of the voltage step (Fig. 1*E*).

**Functional and Pharmacological Properties of $K_V7.2$ and/or $K_V7.3$ Heteromeric Channels Incorporating Mutant $K_V7.2$ R6W and R6Q Subunits.** To evaluate the possible functional changes caused by $K_V7.2$ R6W and $K_V7.2$ R6Q mutant subunits in heteromeric assembly with $K_V7.2$ and/or $K_V7.3$ subunits, CHO cells were transfected with $K_V7.2$+$K_V7.3$ cDNAs at a 1:1 ratio to mimic the genetic balance of normal individuals, and with $K_V7.2$+$K_V7.2$ R6W+$K_V7.3$ or $K_V7.2$+$K_V7.2$ R6Q+$K_V7.3$ (each at 0.5:0.5:1 ratio) to mimic the genetic balance of individuals who carried the mutant $K_V7.2$ alleles in heterozygosity.

Incorporation of $K_V7.3$ subunits into $K_V7.2$+$K_V7.3$ heteromeric channels generated currents with larger size and a reduced sensitivity to the pore blocker tetraethylammonium (TEA) than $K_V7.2$ homomers (Table 1) (1, 16). Compared with $K_V7.2$+$K_V7.3$-transfected cells, cells transfected with $K_V7.2$+$K_V7.2$ R6W+$K_V7.3$ or $K_V7.2$+$K_V7.2$ R6Q+$K_V7.3$ cDNAs generated $K^+$ currents of identical size and TEA sensitivity, suggesting that these mutations failed to interfere with heteromeric subunit assembly (Table 1). By contrast, as in homomeric configuration, heteromeric channels carrying mutations at the R6 residue in $K_V7.2$ displayed a reduced voltage sensitivity (Table 1), with a larger degree of functional impairment in the currents recorded from $K_V7.2$+$K_V7.2$ R6Q+$K_V7.3$- compared with $K_V7.2$+$K_V7.2$ R6W+$K_V7.3$-transfected cells; in fact, the $V_{1/2}$ values were right-shifted by approximately +9 mV and +16 mV in R6W- and R6Q-expressing cells, respectively (Fig. 2*B* and Table 1). Assuming similar transcription/translation efficiency of WT and mutant cDNAs and random assembly of $K_V7.2$ and $K_V7.3$ subunits (17), the majority of channels formed in the described heteromeric configuration incorporated a single mutant subunit. When comparing the functional changes observed in homomeric channels (carrying four mutant subunits) with those in the described heteromeric configuration, the extent of decreased voltage sensitivity appears proportional to the number of mutant subunits incorporated. This seems consistent with the results in which heteromeric channels formed by $K_V7.2$ R6W+$K_V7.3$ or $K_V7.2$ R6Q+$K_V7.3$ channels (mostly containing two mutant subunits per channel) showed an intermediated phenotype, with $V_{1/2}$ shifts of +26 mV and +37 mV, respectively (Table 1).

Given that homomeric $K_V7.2$ channels might contribute to $I_{KM}$ diversity at some neuronal sites (18–20) and might be more prevalent during early development (21), the effects of both R6 $K_V7.2$ mutations were also studied in heteromeric configuration with only $K_V7.2$ subunits (1:1 ratio). Under this experimental condition, which generated a larger proportion of channels

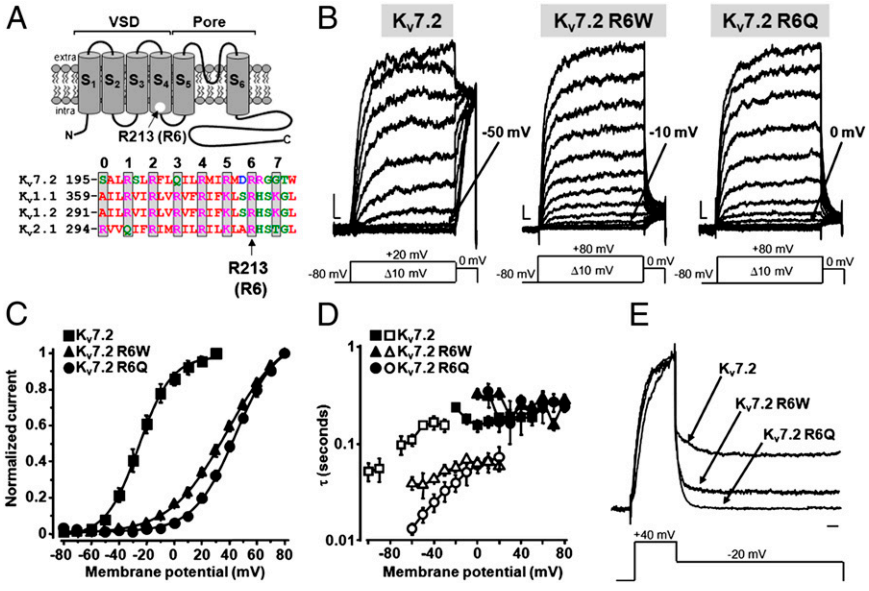


**Fig. 1.** Functional properties of homomeric $K_V7.2$, $K_V7.2$ R6W, and $K_V7.2$ R6Q channels. (*A*) (*Upper*) Topological representation of a $K_V7.2$ subunit. The R213 (R6) residue is highlighted. (*Lower*) Sequence alignment of the $S_4$ segments of the indicated $K_v$ subunits (www.ebi.ac.uk/Tools/psa/). Residues are colored according to the following scheme: magenta, basic; blue, acid; red, nonpolar; and green, polar. (*B*) Macroscopic currents from $K_V7.2$, $K_V7.2$ R6W, and $K_V7.2$ R6Q channels, in response to the indicated voltage protocols. Current scale, 100 pA; time scale, 0.1 s. The arrows indicate the threshold voltage for current activation. (*C*) Conductance/voltage curves. Continuous lines are Boltzmann fits to the experimental data. (*D*) Time constants for ionic current activation (weighed average of $\tau_f$ and $\tau_s$; filled symbols) and deactivation (empty symbols) for the indicated channels ($n$ = 4–9). (*E*) Normalized and superimposed current traces from $K_V7.2$, $K_V7.2$ R6W, and $K_V7.2$ R6Q channels. Current scale, 100 pA; time scale, 100 ms.

**Table 1. Gating and pharmacological properties of $K_V7.2$, $K_V7.2$ R6W, and $K_V7.2$ R6Q subunits in homomeric and heteromeric configuration with $K_V7.2$ and/or $K_V7.3$**

| Subunit | *n* | $V_{1/2}$, mV | *k*, fold mV/*e* | Current density, pA/pF | 3 mM TEA, % of block | Retigabine, ΔV |
|---|---|---|---|---|---|---|
| $K_V7.2$ | 14 | −22.9 ± 1.8 | 12.3 ± 0.6 | 25.9 ± 3.8 (0 mV) | 89.0 ± 2 | ND |
| $K_V7.2$ R6W | 12 | 35.4 ± 4.6*,† | 23.5 ± 2.1*,† | 24.8 ± 4.5 (+60 mV) | ND | ND |
| $K_V7.2$ R6Q | 9 | 45.0 ± 1.9* | 16.6 ± 1.1* | 33.9 ± 8.1 (+60 mV) | ND | ND |
| $K_V7.2$ R6E | 12 | 101.2 ± 4.7*,† | 20.1 ± 1.8* | 51.0 ± 11.0 (+120 mV) | ND | ND |
| $K_V7.2$+$K_V7.2$ R6W | 6 | −6.8 ± 3.1*,‡ | 16.7 ± 1.7*,‡ | 33.3 ± 13.1 (+40 mV) | ND | ND |
| $K_V7.2$+$K_V7.2$ R6Q | 8 | 17.7 ± 3.3* | 19.3 ± 1.0* | 23.6 ± 3.8 (+40 mV) | ND | ND |
| $K_V7.2$+$K_V7.3$ | 17 | −30.7 ± 1.4 | 11.7 ± 0.7 | 110.8 ± 20.7* (0 mV) | 44.6 ± 5.1* | −26.1 ± 1.4 (10 μM);−9.1 ± 2.4 (1 μM) |
| $K_V7.2$ R6W+$K_V7.3$ | 7 | −4.4 ± 4.0§,¶ | 18.0 ± 1.2§ | 92.1 ± 13.7* (+40 mV) | 46.8 ± 6.4* | −24.6 ± 0.8 (10 μM) |
| $K_V7.2$ R6Q+$K_V7.3$ | 14 | 6.7 ± 2.7§ | 20.2 ± 0.9§ | 62.8 ± 9.3* (+40 mV) | 45.6 ± 5.7* | −31 ± 1.2 (10 μM) |
| $K_V7.2$+$K_V7.2$ R6W+$K_V7.3$ | 15 | −22.2 ± 2.0§,‖ | 15.2 ± 1.3§ | 98.8 ± 12.5* (+40 mV) | 45.8 ± 9.2* | −12.7 ± 1.1(1 μM) |
| $K_V7.2$+$K_V7.2$ R6Q+$K_V7.3$ | 12 | −14.7 ± 2.6§ | 14.6 ± 2.6§ | 85.0 ± 17.9* (+4 0mV) | 45.0 ± 5.4* | −11.3 ± 1.3 (1 μM) |

$P < 0.05$ vs. the corresponding value in: *$K_V7.2$, †$K_V7.2$ R6Q, ‡$K_V7.2$+$K_V7.2$ R6Q, §$K_V7.2$+$K_V7.3$, ¶$K_V7.2$ R6Q+$K_V7.3$, and ‖$K_V7.2$+$K_V7.2$ R6Q+$K_V7.3$. ND, not determined.

containing two mutant subunits, the gating changes observed were intermediate between homomeric (four mutant subunits) and single heteromeric subunits (Table 1); also under this experimental condition, R6W-containing channels displayed milder gating changes compared with R6Q-substituted channels (Fig. 2*C*).

The functional changes prompted on channel gating by both $K_V7.2$ mutations at position R6 are opposite to those caused by retigabine, a prototypic opener of channel formed by neuronal $K_v7$ subunits (13). In fact, both in native $I_{KM}$ and in heterologously expressed neuronal homomeric or heteromeric $K_V7$ channels, retigabine causes a concentration-dependent shift in the hyperpolarizing direction of the voltage dependence of the channel activation process (Table 1), accompanied by a slower channel deactivation and a variable degree of maximal current potentiation. The effects of retigabine appeared to be unaffected by incorporation of subunits carrying the R6 mutations: in fact, in both $K_V7.2$+$K_V7.2$ R6W+$K_V7.3$ and $K_V7.2$+$K_V7.2$ R6Q+$K_V7.3$ heteromers, retigabine fully reversed mutation-induced gating changes, thereby restoring voltage sensitivity to WT values (Fig. 3 and Table 1). In these experiments, retigabine was used at a concentration (1 μM) close to that achieved in human plasma during conventional oral drug treatment (22), considering a maximum concentration of 500 to 1,500 ng/mL and a plasma protein binding of approximately 80% (13). Higher retigabine concentrations (10 μM) caused a larger hyperpolarizing shift in activation of heteromeric channels, the extent of which was similar in channels containing WT or R6W/Q mutant subunits (Table 1).

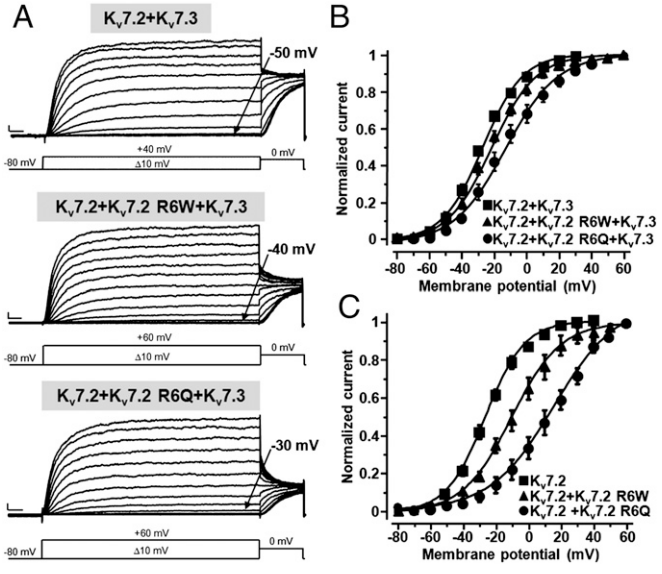


**Fig. 2.** Functional properties of heteromeric channels incorporating $K_V7.2$ R6W or $K_V7.2$ R6Q mutant subunits. (*A*) Macroscopic current traces from the indicated heteromeric channels in response to the indicated voltage protocols. Current scale, 200 pA; time scale, 0.1 s The arrows indicate the threshold voltage for current activation. (*B* and *C*) Conductance/voltage curves for the heteromeric channels formed by mutant subunits with $K_V7.2$ and $K_V7.3$ (*B*) or with $K_V7.2$ (*C*). Continuous lines are Boltzmann fits to the experimental data. The cDNA ratios were: 1:1 for $K_V7.2$+$K_V7.3$, $K_V7.2$+$K_V7.2$ R6W, and $K_V7.2$+$K_V7.2$ R6Q, and 0.5:0.5:1 for $K_V7.2$+$K_V7.2$ R6W+$K_V7.3$ and $K_V7.2$+$K_V7.2$ R6Q+$K_V7.3$. Current scale, 200 pA; time scale, 100 ms.

**Computational Modeling.** To test the possible functional effects of the described gating changes on intrinsic neuronal excitability, a series of simulations were run after incorporation of the kinetic (activation/deactivation) and steady-state parameters experimentally derived from $K_V7.2$+$K_V7.3$, $K_V7.2$+$K_V7.2$ R6W+$K_V7.3$, or $K_V7.2$+$K_V7.2$ R6Q+$K_V7.3$ heteromeric channels into a model CA1 hippocampal neuron. The number of APs was calculated from 500-ms-long simulations, as a function of somatic current injections and peak $I_{KM}$ conductances. Typical voltage responses and expanded sweep displays of the activated conductances from control or mutant model cells during a 0.65-nA somatic current injection and 120 pS/μm$^2$ for $I_{KM}$ are shown in Fig. 4 *A* and *B*, respectively. When AP number was studied across a wide range of injected current (between 0.3 and 0.7 nA), it was found that, whereas R6Q mutant cells responded with a much higher number of spikes compared with control cells at relatively low current injection values, R6W produced similar effects only for larger input currents (Fig. 4*C*). It is noteworthy that such a dramatic difference between R6Q and R6W mutants, as well as between both mutants and WT channels, was observed across a wide range of peak $I_{KM}$ conductances (between 0 and 170 pS/μm$^2$; Fig. 4*D*). A strong mutation-induced increase in cell excitability, with more dramatic effects prompted by R6Q compared with R6W, was also observed when computer simulation were run under the following experimental conditions: (*i*) when somatic and axonal $I_{KM}$ incorporated the kinetic and steady-state parameters experimentally derived from $K_V7.2$, Kv7.2/Kv7.2R6W, and Kv7.2/Kv7.2R6Q heteromers (Fig. S1); (*ii*) when parameters from Kv7.2/Kv7.3 heteromers were included to model the somatic component of the $I_{KM}$, whereas data for Kv7.2 homomers were used to model the axonal $I_{KM}$ (Fig. S2); and (*iii*) when model parameters were modified to generate bursting behavior upon $I_{KM}$ blockade (Fig. S3).

## Discussion

In humans, gene defects in *$K_V7.2$* cause neonatal epilepsies characterized by a wide phenotypic heterogeneity. In fact, mutations

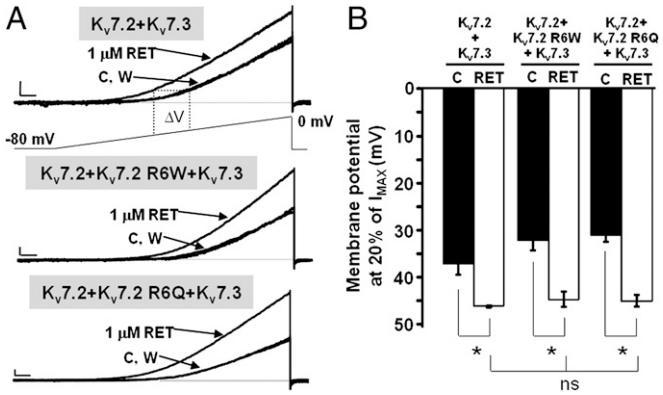


**Fig. 3.** Effect of retigabine on heteromeric $K_V7.2+K_V7.3$, $K_V7.2+K_V7.2$ R6W+$K_V7.3$, or $K_V7.2+K_V7.2$ R6Q+$K_V7.3$ channels. (*A*) Current responses from the indicated heteromeric channels to voltage ramps from −80 to 0 mV. C, control currents; RET, retigabine; W, washout. Current scale, 200 pA; time scale, 0.2 s. (*B*) Quantification of the effects of RET on the indicated heteromeric channels. Data are expressed as membrane potentials at which currents reached 20% of their peak value for controls (black bars) and after RET exposure (white bars). *$P < 0.05$ vs. corresponding controls; ns, not significantly different). Current scale, 200 pA; time scale, 200 ms.

in $K_V7.2$ (5, 6) and, more rarely, $K_V7.3$ (7) genes are well-known causes of BFNS, a dominantly inherited neonatal epilepsy with mostly favorable outcome. More recently, novel $K_V7.2$ mutations have been identified in children with severe forms of neonatal-onset epileptic encephalopathies (8, 9), characterized by distinct EEG and MRI features, and variable degrees of psychomotor delays. Noteworthy, familial cases with more severe neurodevelopmental outcome have also been described in BFNS families carrying $K_v7.2$ mutations (23–25).

Although the molecular basis for this striking phenotypic variability is yet unknown, differences in the functional effects caused by the specific amino acid substitutions have been suggested as a plausible explanation (8). Therefore, in the present study, we have investigated the molecular pathogenesis of channel dysfunction caused by two mutations affecting the same residue in the VSD of $K_V7.2$, which are responsible for "$K_V7.2$ epileptic encephalopathy" (R6Q) (8), or for BFNS (R6W) (12). Macroscopic current analysis in transfected cells revealed that both mutations, in homomeric or heteromeric configuration with $K_V7.2$ and/or $K_V7.3$, did not modify the maximal density of the expressed currents, suggesting that channel trafficking to the plasma membrane was unaffected; instead, homomeric R6Q mutant $K_v1.1$ channels were nonfunctional because of a maturation deficit (26). More importantly, channels carrying either $K_V7.2$ mutation at R6 showed a remarkable decrease in their voltage sensitivity, with the R6Q mutation prompting more dramatic effects compared with the R6W mutation. For both mutations, the extent of gating impairment appeared proportional to the number of mutant subunits incorporated, being maximal in homomeric configuration (four mutant subunits), intermediate in channels mostly containing two mutant subunits (in homomeric configuration with $K_V7.2$ subunits or in heteromeric configuration with $K_V7.3$ subunits), and smaller in heteromeric channels reproducing the genetic balance of affected individuals (mostly containing a single mutant subunit). R6 is not believed to contribute directly to gating charge movement, a function mainly attributed to the first four positively charged residues in $S_4$ (27); nevertheless, the reduced voltage sensitivity of channels carrying R6 mutations appears as a consequence of a decreased stability of the activated VSD configuration, as revealed by the faster and more complete deactivation, with no appreciable difference in activation kinetics. Of note, a crucial role for the R6 residue in stabilizing the activated configuration of the VSD and in the electromechanical coupling between VSD repositioning and pore opening (28) has also been recently revealed from gating current measurements in highly homologous $K_V7.4$ channels (29).

A mild decrease of $I_{KM}$ function appears sufficient to cause BFNS, and haploinsufficiency seems to be the primary pathogenetic mechanism for familial and sporadic cases of BFNS. Such mild $I_{KM}$ impairment can be caused by mutations decreasing expression, intracellular trafficking, polarized targeting, or voltage sensitivity of $K_v7.2$ subunits (30). The R6 mutations described here seem to be within this latter group. However, the R6W mutation caused gating changes qualitatively and quantitatively similar to those of previously described BFNS mutations (14, 15, 31, 32). By contrast, the 16-mV positive shift in $V_{1/2}$ observed upon incorporation of a single $K_V7.2$ R6Q subunit in heteromeric configuration with $K_V7.2$ and $K_V7.3$ subunits to recapitulate the genotype of the individual affected with $K_V7.2$ encephalopathy (8), is the most dramatic among the functional changes described in $K_V7.2$ channelopathies (33). More dramatic effects of the R6Q mutation compared with the R6W mutation were also observed in homomeric $K_V7.2$ channels, which have been suggested to contribute to $I_{KM}$ diversity at Ranvier nodes in central and peripheral fibers (18, 19) and, possibly, presynaptic nerve terminals (20). Notably, in rat superior cervical ganglion neurons, $K_v7.2$ homomers appear to be

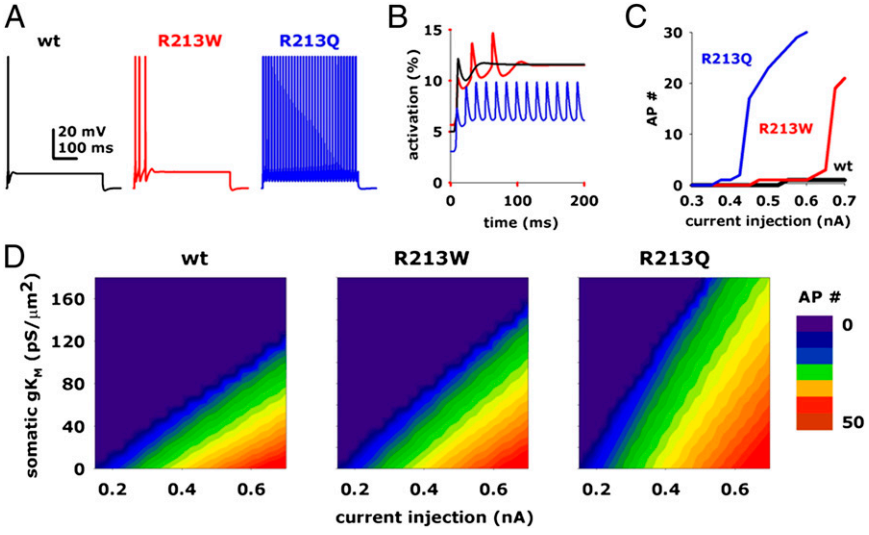


**Fig. 4.** Modeling of the effects of the $K_V7.2$ R213W (R6W) and R213Q (R6Q) mutations on neuronal excitability. Time courses of the somatic membrane potential (*A*) and of the activated conductances (*B*; only the first 200 ms are shown) from CA1 neurons expressing $K_V7.2+K_V7.3$ (black traces), $K_V7.2+K_V7.2$ R6W+$K_V7.3$ (red traces), or $K_V7.2+K_V7.2$ R6Q+$K_V7.3$ (blue traces) heteromeric channels, during a 500-ms somatic current injection of 0.65 nA. (*C*) Input/output (I/O) curves from cells expressing $K_V7.2+K_V7.3$ (black trace), $K_V7.2+K_V7.2$ R6W+$K_V7.3$ (red trace), or $K_V7.2+K_V7.2$ R6Q+$K_V7.3$ (blue trace) heteromeric channels. Number of APs (AP#) is expressed as a function of the somatic current injected, using a 120 mS/μm$^2$ peak $I_{KM}$ conductance. (*D*) Contour plots for number of APs elicited by a 500-ms somatic current injection from cells expressing $K_V7.2+K_V7.3$, $K_V7.2+K_V7.2$ R6W+$K_V7.3$, or $K_V7.2+K_V7.2$ R6Q+$K_V7.3$ heteromeric channels as a function of current injection and peak $I_{KM}$ conductance.

more prevalent during early development (21). Computational results in a CA1 hippocampal model neuron revealed that, in heteromeric configuration with $K_V7.2$ and $K_V7.3$ subunits, incorporation of a single R6Q and, to a lesser extent, R6W subunit markedly increased neuronal excitability. Similarly, Peters et al. (34) showed that $I_{KM}$-deficient CA1 pyramidal cells displayed no change in AP parameters, but showed increased excitability and reduced spike-frequency adaptation after depolarizing current injection. The results obtained, which showed that the $K_V7.2$ encephalopathy-associated R6Q mutation prompted gating alterations significantly more pronounced than the BFNS-associated R6W mutation, suggest that the extent of mutation-induced functional impairment may be related to the clinical severity of the disease, thus uncovering unique genotype–phenotype correlations in $K_V7.2$-linked channelopathies.

The observation that more dramatic functional changes were found when R6 was substituted by a Q rather than by a W is somehow surprising because, even though both amino acids lack the positive charge, Q has a similar size to R, whereas W is considerably bulkier. To achieve a better understanding of the role of the R6 residue in channel gating, and to provide a plausible structural hypothesis to explain the mutation-induced functional changes, we built a homology model of the $K_V7.2$ subunit (11) based on the crystal structure of the open configuration of a $K_v1.2/K_v2.1$ chimeric channel (35) (Fig. 5*A*). In this model, the activated VSD configuration is stabilized by electrostatic interactions between $S_4$ positively charged residues and negative charges provided by the $S_1$–$S_2$ linker (32) and both $S_2$ and $S_3$ segments. In particular, R207 (R4) forms a salt bridge with E130 in $S_2$, an interaction stabilized by $K_V7$ activators acting as gating modifiers (36). On the contrary, R210 (R5) and R213 (R6) form ionized hydrogen bonds with an internal negative amino acid cluster mostly provided by E140 in $S_2$ and D172 in $S_3$ (11, 15); in particular, R6 interacts with D172 in $S_3$ (Fig. 5*B*). The replacement of R6 with a Q (Fig. 5*C*) impeded such electrostatic interactions, possibly destabilizing the VSD activated configuration; the fact that charge reversal at the R6 residue (R6E; Fig. 5*D*) caused even more dramatic gating changes compared with the R6Q charge neutralization (Table 1), is in line with this hypothesis. By contrast, the introduction of a W residue at R6, although also occluding the ionized hydrogen bonds with the internal cluster of negative charges, may bring about a π-stacking interaction with a neighbor F168 residue in $S_3$ (Fig. 5*E*); such an interaction, although weaker than the ionized hydrogen bond in $K_V7.2$ subunits (37), may provide a certain degree of VSD stabilization, thereby resulting in more subtle functional effects. The fact that the functional differences between R6W and R6Q mutations were largely prevented upon replacement of F168 with a nonaromatic leucine (Figs. S4–S6) seems in line this hypothesis.

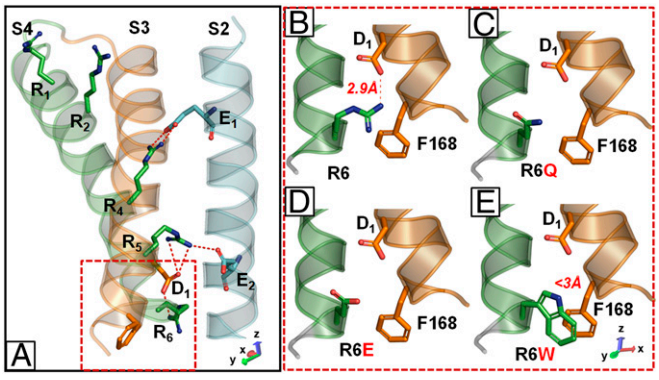


**Fig. 5.** Homology models of $K_V7.2$, $K_V7.2$ R6W, $K_V7.2$ R6Q, and $K_V7.2$ R6E subunits. (*A*) Homology model of activated configuration of VSD of a single $K_V7.2$ subunit; only $S_2$, $S_3$, and $S_4$ segments are shown for clarity. Charged amino acids shown correspond to E130 (E1) and E140 (E2) in $S_2$, D172 (D1) in $S_3$, and R198 (R1), R201 (R2), R207 (R4), R210 (R5), and R213 (R6) in $S_4$. (*B–E*) Higher magnification of the boxed region in *A* in a single $K_V7.2$ (*B*), $K_V7.2$ R6Q (*C*), $K_V7.2$ R6E (*D*), and $K_V7.2$ R6W (*E*) subunit. To improve clarity, images in *B–E* are shown after leftward rotation by 90° of the model shown in *A*.

Although the present results do not cover the full spectrum of possible mutation-induced channel dysfunction, and the severity of the disease is likely influenced by additional, yet unknown environmental and genetic risk factors, the present data provide evidence for a major pathogenetic role of the described gating changes in phenotypic expression of $K_V7.2$ channelopathies. Moreover, the presently described genotype–phenotype correlations might have relevant impact on disease-management procedures (i.e., for early genotyping) and on clinical course prediction. In fact, neonatal seizures can be harmful to the developing brain in experimental animals, and, possibly, in humans (38). In fact, seizure severity appears as an indicator of subsequent neurodevelopmental outcome in children with hypoxic-ischemic encephalopathy (39), and early recognition and treatment of seizures can reduce brain injury in newborns with hypoxic-ischemic encephalopathy (40).

Safer and more effective treatments for neonatal seizures are strongly needed. First-line drugs (mostly phenobarbital and phenytoin) are effective in fewer than 50% of cases (41), and experimental data have raised concerns about the potential adverse effects on brain development of anticonvulsant agents currently used in neonates (42). Animal studies have previously highlighted $K_v7/I_{KM}$ channels as targets for neonatal seizure treatment (43). The present results indicate that the neuronal $K_v7/I_{KM}$ opener retigabine, at clinically relevant concentrations (13, 22), was able to restore normal function in channels carrying $K_V7.2$ subunits mutated at the R6 position, thereby setting the preclinical basis for the potential use of $K_v7/I_{KM}$ openers as a targeted therapy for neonatal seizures and to improve the developmental outcome of neonates with $K_V7.2$ encephalopathy.

## Materials and Methods

**Mutagenesis of $K_V7.2$ cDNA and Heterologous Expression of WT and Mutant $K_V7.2$ cDNAs.** Mutations were engineered in human $K_V7.2$ cDNA cloned into pcDNA3.1 by sequence overlap extension PCR with the *Pfu* DNA polymerase as described previously (15). Channel subunits were expressed in CHO cells by transient transfection using Lipofectamine 2000 (Invitrogen) according to the manufacturer's protocol. A plasmid encoding for EGFP (Clontech) was used as transfection marker.

**Whole-Cell Electrophysiology.** Currents from CHO cells were recorded at room temperature (20–22 °C) 1 to 2 d after transfection by using an Axopatch 200A (Molecular Devices) and the whole-cell configuration of the patch-clamp technique, with glass micropipettes of 3 to 5 MΩ resistance. The extracellular solution contained (in mM) 138 NaCl, 2 $CaCl_2$, 5.4 KCl, 1 $MgCl_2$, 10 glucose, and 10 Hepes, pH 7.4 adjusted with NaOH; the pipette (intracellular) solution contained (in mM) 140 KCl, 2 $MgCl_2$, 10 EGTA, 10 Hepes, 5 Mg-ATP, pH 7.3 to 7.4 adjusted with KOH. pCLAMP software (version 10.0.2) was used for data acquisition and analysis. Currents were corrected offline for linear capacitance and leakage currents by using standard subtraction routines (Clampfit module of pClamp 10). No corrections were made for liquid junction potentials.

To generate conductance–voltage curves, the cells were held at −80 mV, then depolarized for 1.5 s from −80 mV to +20/+120 mV in 10-mV increments, followed by an isopotential pulse at 0 mV of 300 ms duration. Current values at the beginning of the 0-mV pulse were measured, normalized, expressed as a function of the preceding voltages, and fitted to a Boltzmann distribution of the form $y = max/[1 + exp(V_{1/2} - V)/k]$ to obtain $V_{1/2}$ and slope factor $k$. Current traces were fit to a single- or a double-exponential function; in the latter case, a single time constant representing the weighted average of the slow and fast components was obtained by using the following equation: $\tau = (\tau_f A_f + \tau_s A_s)/(A_f + A_s)$.

In the experiments with TEA or retigabine (obtained from Valeant Pharmaceuticals, Aliso Viejo, CA) currents were activated by 3-s voltage ramps from −80 mV to 0 mV at 0.08-Hz frequency. TEA blockade was expressed as the percentage of peak current inhibition produced by a 2-min drug application; the effects of retigabine were expressed as the negative

shift in the ramp voltage at which the currents reached 20% of their peak value after 2-min drug application.

**Computational Modeling.** All simulations were carried out with the NEURON program, version 7 (44), by using a previously described 3D model of a CA1 pyramidal neuron (45). Uniform passive properties were used over the entire neuron, with $C_m$ of 0.75 μF/cm$^2$ and $R_m$ of 37.3 kΩ/cm$^2$ ($\tau_m$ = 28 ms). Active somatic and dendritic properties included the following conductances: sodium ($I_{Na}$), potassium delayed rectifier ($I_{DR}$), potassium transient ($I_A$), potassium M ($I_{KM}$), and nonselective, hyperpolarization-activated ($I_h$); a low-threshold $Ca^{2+}$ and a $Ca^{2+}$-dependent $K^+$ conductance, as well as a simple $Ca^{2+}$ extrusion mechanism, were also included. $I_{Na}$, $I_{DR}$, $Ca^{2+}$-, and $Ca^{2+}$-dependent $K^+$ conductances were included at uniform density over the somatodendritic region, and $I_A$ and $I_h$ linearly increasing with distance from the soma. $I_{KM}$-generating $K_v7$ channels are mostly concentrated at the axon initial segment (45, 46); therefore, the data shown in Fig. 4 were obtained with a threefold larger density of $I_{KM}$ within the axonal over the somatic compartment (45). $I_{KM}$ peak conductances (0–170 pS/μm$^2$) refer to somatic values. The $I_{KM}$ properties were implemented to fit the steady-state and kinetic values obtained in this work. The complete model and simulation files are available for public download under the ModelDB section of the Senselab database (http://senselab.med.yale.edu/modeldb/) (47).

**Homology Modeling.** Three-dimensional models of $K_v7.2$ subunits were generated by homology modeling by using SWISS-MODEL (11, 48). A chimeric channel in which the voltage-sensor paddle (corresponding to the $S_{3b}$–$S_4$ region) of $K_v2.1$ was transferred into the $K_v1.2$ subunit (35) was used as template (PDB ID code 2R9RH). The model was optimized through all-atom energy minimization process by using the GROMOS96 implementation of Swiss-PDBViewer, and analyzed by using both the DeepView module of Swiss-PDBViewer (version 4.0.1; http://spdbv.vital-it.ch/) and PyMOL (http://www.pymol.org/).

**Statistics.** Data are expressed as mean ± SEM. Statistically significant differences were evaluated with the Student *t* test or with ANOVA followed by the Student–Newman–Keuls test, with the threshold set at $P < 0.05$.

**ACKNOWLEDGMENTS.** We thank Prof. Thomas J. Jentsch (Max Delbrück Center for Molecular Medicine, Berlin, Germany) for $K_V7.2$ and $K_V7.3$ cDNAs. This study was supported by Telethon Grant GGP07125 (to M.T.), Neuroscience Program of the Compagnia di San Paolo (M.T.), Regione Molise Convenzione Agenzia Italiana del Farmaco/Regione Molise (M.T.), Science and Technology Council of the Province of Avellino (M.T.), Programmi di Ricerca di Rilevante interesse Nazionale 2009 (M.T.), and E-Rare Joint Transnational Call 2007 (to M.R.C. and M.T.).

1. Wang HS, et al. (1998) KCNQ2 and KCNQ3 potassium channel subunits: Molecular correlates of the M-channel. *Science* 282(5395):1890–1893.
2. Brown DA, Adams PR (1980) Muscarinic suppression of a novel voltage-sensitive K+ current in a vertebrate neurone. *Nature* 283(5748):673–676.
3. Soldovieri MV, Miceli F, Taglialatela M (2011) Driving with no brakes: Molecular pathophysiology of Kv7 potassium channels. *Physiology (Bethesda)* 26(5):365–376.
4. Cooper EC, Harrington E, Jan YN, Jan LY (2001) M channel KCNQ2 subunits are localized to key sites for control of neuronal network oscillations and synchronization in mouse brain. *J Neurosci* 21(24):9529–9540.
5. Biervert C, et al. (1998) A potassium channel mutation in neonatal human epilepsy. *Science* 279(5349):403–406.
6. Singh NA, et al. (1998) A novel potassium channel gene, KCNQ2, is mutated in an inherited epilepsy of newborns. *Nat Genet* 18(1):25–29.
7. Charlier C, et al. (1998) A pore mutation in a novel KQT-like potassium channel gene in an idiopathic epilepsy family. *Nat Genet* 18(1):53–55.
8. Weckhuysen S, et al. (2012) KCNQ2 encephalopathy: emerging phenotype of a neonatal epileptic encephalopathy. *Ann Neurol* 71(1):15–25.
9. Saitsu H, et al. (2012) Whole exome sequencing identifies KCNQ2 mutations in Ohtahara syndrome. *Ann Neurol* 72(2):298–300.
10. Nabbout R, Dulac O (2011) Epilepsy. Genetics of early-onset epilepsy with encephalopathy. *Nat Rev Neurol* 8(3):129–130.
11. Miceli F, et al. (2008) Gating consequences of charge neutralization of arginine residues in the S4 segment of K(v)7.2, an epilepsy-linked K+ channel subunit. *Biophys J* 95(5):2254–2264.
12. Sadewa AH, et al.; Gunadi (2008) Germ-line mutation of KCNQ2, p.R213W, in a Japanese family with benign familial neonatal convulsion. *Pediatr Int* 50(2):167–171.
13. Gunthorpe MJ, Large CH, Sankar R (2012) The mechanism of action of retigabine (ezogabine), a first-in-class K+ channel opener for the treatment of epilepsy. *Epilepsia* 53(3):412–424.
14. Castaldo P, et al. (2002) Benign familial neonatal convulsions caused by altered gating of KCNQ2/KCNQ3 potassium channels. *J Neurosci* 22(2):RC199.
15. Miceli F, et al. (2009) Neutralization of a unique, negatively-charged residue in the voltage sensor of K V 7.2 subunits in a sporadic case of benign familial neonatal seizures. *Neurobiol Dis* 34(3):501–510.
16. Soldovieri MV, et al. (2006) Decreased subunit stability as a novel mechanism for potassium current impairment by a KCNQ2 C terminus mutation causing benign familial neonatal convulsions. *J Biol Chem* 281(1):418–428.
17. Stewart AP, et al. (2012) The Kv7.2/Kv7.3 heterotetramer assembles with a random subunit arrangement. *J Biol Chem* 287(15):11870–11877.
18. Devaux JJ, Kleopa KA, Cooper EC, Scherer SS (2004) KCNQ2 is a nodal K+ channel. *J Neurosci* 24(5):1236–1244.
19. Schwarz JR, et al. (2006) KCNQ channels mediate IKs, a slow K+ current regulating excitability in the rat node of Ranvier. *J Physiol* 573(Pt 1):17–34.
20. Martire M, et al. (2004) M channels containing KCNQ2 subunits modulate norepinephrine, aspartate, and GABA release from hippocampal nerve terminals. *J Neurosci* 24(3):592–597.
21. Hadley JK, et al. (2003) Stoichiometry of expressed KCNQ2/KCNQ3 potassium channels and subunit composition of native ganglionic M channels deduced from block by tetraethylammonium. *J Neurosci* 23(12):5012–5019.
22. Hermann R, et al. (2003) Effects of age and sex on the disposition of retigabine. *Clin Pharmacol Ther* 73(1):61–70.
23. Borgatti R, et al. (2004) A novel mutation in KCNQ2 associated with BFNC, drug resistant epilepsy, and mental retardation. *Neurology* 63(1):57–65.
24. Dedek K, Fusco L, Teloy N, Steinlein OK (2003) Neonatal convulsions and epileptic encephalopathy in an Italian family with a missense mutation in the fifth transmembrane region of KCNQ2. *Epilepsy Res* 54(1):21–27.
25. Steinlein OK, Conrad C, Weidner B (2007) Benign familial neonatal convulsions: Always benign? *Epilepsy Res* 73(3):245–249.
26. Papazian DM, et al. (1995) Electrostatic interactions of S4 voltage sensor in Shaker K+ channel. *Neuron* 14(6):1293–1301.
27. Aggarwal SK, MacKinnon R (1996) Contribution of the S4 segment to gating charge in the Shaker K+ channel. *Neuron* 16(6):1169–1177.
28. Long SB, Campbell EB, Mackinnon R (2005) Voltage sensor of Kv1.2: Structural basis of electromechanical coupling. *Science* 309(5736):903–908.
29. Miceli F, Vargas E, Bezanilla F, Taglialatela M (2012) Gating currents from Kv7 channels carrying neuronal hyperexcitability mutations in the voltage-sensing domain. *Biophys J* 102(6):1372–1382.
30. Maljevic S, Wuttke TV, Lerche H (2008) Nervous system KV7 disorders: Breakdown of a subthreshold brake. *J Physiol* 586(7):1791–1801.
31. Dedek K, et al. (2001) Myokymia and neonatal epilepsy caused by a mutation in the voltage sensor of the KCNQ2 K+ channel. *Proc Natl Acad Sci USA* 98(21):12272–12277.
32. Wuttke TV, et al. (2008) Neutralization of a negative charge in the S1-S2 region of the KV7.2 (KCNQ2) channel affects voltage-dependent activation in neonatal epilepsy. *J Physiol* 586(2):545–555.
33. Bellini G, et al. (2010) Benign familial neonatal seizures. *GeneReviews*, eds Pagon RA, Bird TD, Dolan CR, Stephens K (Univ Washington, Seattle). Available at http://www.ncbi.nlm.nih.gov/books/NBK32534/.
34. Peters HC, Hu H, Pongs O, Storm JF, Isbrandt D (2005) Conditional transgenic suppression of M channels in mouse brain reveals functions in neuronal excitability, resonance and behavior. *Nat Neurosci* 8(1):51–60.
35. Long SB, Tao X, Campbell EB, MacKinnon R (2007) Atomic structure of a voltage-dependent K+ channel in a lipid membrane-like environment. *Nature* 450(7168):376–382.
36. Peretz A, et al. (2010) Targeting the voltage sensor of Kv7.2 voltage-gated K+ channels with a new gating-modifier. *Proc Natl Acad Sci USA* 107(35):15637–15642.
37. Burley SK, Petsko GA (1985) Aromatic-aromatic interaction: A mechanism of protein structure stabilization. *Science* 229(4708):23–28.
38. Chapman KE, Raol YH, Brooks-Kayal A (2012) Neonatal seizures: Controversies and challenges in translating new therapies from the lab to the isolette. *Eur J Neurosci* 35(12):1857–1865.
39. Glass HC, et al. (2009) Clinical neonatal seizures are independently associated with outcome in infants at risk for hypoxic-ischemic brain injury. *J Pediatr* 155(3):318–323.
40. van Rooij LG, et al. (2010) Effect of treatment of subclinical neonatal seizures detected with aEEG: Randomized, controlled trial. *Pediatrics* 125(2):e358–e366.
41. Painter MJ, et al. (1999) Phenobarbital compared with phenytoin for the treatment of neonatal seizures. *N Engl J Med* 341(7):485–489.
42. Sankar R, Painter MJ (2005) Neonatal seizures: After all these years we still love what doesn't work. *Neurology* 64(5):776–777.
43. Raol YH, Lapides DA, Keating JG, Brooks-Kayal AR, Cooper EC (2009) A KCNQ channel opener for experimental neonatal seizures and status epilepticus. *Ann Neurol* 65(3):326–336.
44. Hines ML, Carnevale NT (1997) The NEURON simulation environment. *Neural Comput* 9(6):1179–1209.
45. Chung HJ, Jan YN, Jan LY (2006) Polarized axonal surface expression of neuronal KCNQ channels is mediated by multiple signals in the KCNQ2 and KCNQ3 C-terminal domains. *Proc Natl Acad Sci USA* 103(23):8870–8875.
46. Shah MM, Migliore M, Valencia I, Cooper EC, Brown DA (2008) Functional significance of axonal Kv7 channels in hippocampal pyramidal neurons. *Proc Natl Acad Sci USA* 105(22):7869–7874.
47. Migliore M, et al. (2003) ModelDB: Making models publicly accessible to support computational neuroscience. *Neuroinformatics* 1(1):135–139.
48. Schwede T, Kopp J, Guex N, Peitsch MC (2003) SWISS-MODEL: An automated protein homology-modeling server. *Nucleic Acids Res* 31(13):3381–3385.